frontiers in Materials

ORIGINAL RESEARCH
published: 23 September 2020
doi: 10.3389/fmats.2020.00296

The Influence of Mo Additions on the Microstructure and Mechanical Properties of $AlCrFe_2Ni_2$ Medium Entropy Alloys

Sergej Gein, Victor T. Witusiewicz and Ulrike Hecht*

Access e.V., Aachen, Germany

The alloy system Al-Cr-Fe-Ni provides means for developing novel duplex materials composed of face-centered cubic (FCC) and body-centered cubic (BCC) phases with nearly equal volume fraction. We performed an alloy development study starting from the medium entropy alloy $AlCrFe_2Ni_2$ and adding small amounts of molybdenum in the following series (at.%): $Al_{17}Cr_{17}Fe_{33}Ni_{33}$, $Al_{17}Cr_{17}Fe_{33}Ni_{33}Mo_1$, $Al_{16}Cr_{16}Fe_{33}Ni_{33}Mo_2$, and $Al_{16}Cr_{16}Fe_{33}Ni_{33}Mo_3$. We focused the research on samples with an ultrafine vermicular duplex microstructure, a unique structure requiring sufficiently high cooling rates to suppress the conventional Widmanstätten colony formation. The samples were produced by arc melting in buttons of 300 g each. We characterized the microstructure of the samples using scanning electron microscopy (SEM), energy-dispersive X-ray spectroscopy (EDS), and electron backscatter diffraction (EBSD). The EBSD data revealed significant strain in the FCC phase resulting from the BCC→FCC phase transformation. We investigated mechanical properties of the samples by micro-indentation and 3-point bending in a miniature testing device. The test specimens were in the as-cast condition, as well as in distinct annealed conditions. Annealing treatments were carried out at 950 and 1100°C under argon. The annealing lasted from 10 min to 6 h, followed by water quenching. Prolonged annealing at 950°C of Mo-containing samples resulted in the formation of sigma-phase. Annealing at 1100°C safely avoided sigma-phase formation, while leading to a good balance between the flexural strength and ductility of these samples. Mechanical testing also included the well-established superduplex steel 1.4517 (DIN EN 10283/ASTM A890) as reference material.

Keywords: duplex microstructure, medium entropy alloys, mechanical properties, spinodal decomposition, sigma-phase, alloy development

OPEN ACCESS

Edited by:
Liqiang Wang,
Shanghai Jiao Tong University, China

Reviewed by:
Zhiming Li,
Central South University, China
Yan Wang,
Xi'an University of Architecture and Technology, China

****Correspondence:***
Sergej Gein
s.gein@access-technology.de

Specialty section:
This article was submitted to Structural Materials, a section of the journal Frontiers in Materials

Received: *29 May 2020*
Accepted: *06 August 2020*
Published: *23 September 2020*

Citation:
Gein S, Witusiewicz VT and Hecht U (2020) The Influence of Mo Additions on the Microstructure and Mechanical Properties of $AlCrFe_2Ni_2$ Medium Entropy Alloys. Front. Mater. 7:296. doi: 10.3389/fmats.2020.00296

INTRODUCTION

In the last two decades, research on high entropy alloys (HEAs) aimed at finding alloys that would allow obtaining single-phase equiatomic HEAs exhibiting face-centered-cubic (FCC), body-centered-cubic (BCC), and hexagonal-close-packed (HCP) structures while eliminating secondary (and tertiary) phases (Kozak et al., 2015; Steurer, 2020). However, in recent years a paradigm shift has taken place that puts the focus on dual-phase (or multi-phase) HEAs and intentionally takes advantage of their heterophase nature to achieve superior mechanical properties

(Bönisch et al., 2018). Furthermore, increasing attention is given to medium entropy alloys with less than five elements, not at least with the aim of avoiding expensive and resource-critical elements like Cobalt (Tkaczyk et al., 2018). This opens opportunities to develop novel materials for industrial applications, whenever clear development targets are set forward. The alloy system Al-(Co)-Cr-Fe-Ni is one interesting candidate for the development of dual phase materials, building on rich knowledge from the ternary subsystems Fe-Cr-Ni (Jönsson, 1995; Wróbel et al., 2015), Fe-Ni-Al (Eleno et al., 2006), etc. These subsystems host the well-known family of duplex steels (Alvarez-Armas and Degallaix-Moreuil, 2013), B2-ordered intermetallic alloys, and a series of eutectic alloys (Misra and Gibala, 1997). The alloy system Al-(Co)-Cr-Fe-Ni also offers means to exploit some features of spinodal decomposition (Langer, 1971) for microstructure tailoring. Novel dual phase materials have been reported in the system Al-(Co)-Cr-Fe-Ni (Dong et al., 2016; Abuzaid and Sehitoglu, 2018; Bönisch et al., 2018; Gwalani et al., 2019; Li C. et al., 2020; Li Z. et al., 2020). Unique so far are vermicular duplex microstructures (Dong et al., 2016; Li C. et al., 2020) composed of an ultrafine vermicular FCC phase intertwined with a spinodally decomposed BCC in nearly equal volume fraction. They were first reported in 2016 by Dong et al. (2016) in an $AlCrFe_2Ni_2$ alloy, being termed "noodle-like" and suggested to be of eutectic origin. Similar microstructures are equally found in Co-containing alloys.

During the exploration of the Al-Cr-Fe-Ni and the Al-Co-Cr-Fe-Ni systems with respect to the addition of further alloying elements, molybdenum was investigated by Hsu et al. (2010), Zhu et al. (2010), and Dong et al. (2013), respectively. Dong et al. (2013) investigated a series of alloys $AlCrFeNiMo_x$ with the molar ratio x ranging from 0 to 1, explicitly $x = 0.0, 0.2, 0.5, 0.8, 1.0$. All alloys $x < 0.5$ displayed BCC-based microstructures. For Mo exceeding $x > 0.5$, the primary phase was identified as sigma phase. Compression tests for $x = 0.2$, corresponding to a Mo content of 4.8 at.–%, revealed fracture strength as high as 3.22 GPa and a plastic strain of 28.7%, however with a cleavage-like appearance of the fracture surface. To our best knowledge, molybdenum additions to the alloy $AlCrFe_2Ni_2$ were not reported in literature, despite the increasing interested in alloys, which form dual-phase microstructures.

In this study, we selected the $AlCrFe_2Ni_2$ alloy to revisit the microstructure and further develop the alloy by minor additions of molybdenum in the range from 1–3 at.–% to the baseline composition. The study encompasses four alloys, that is, $Al_{17}Cr_{17}Fe_{33}Ni_{33}$ (Mo_0), $Al_{17}Cr_{17}Fe_{33}Ni_{33}Mo_1$ (Mo_1), $Al_{16}Cr_{16}Fe_{33}Ni_{33}Mo_2$ (Mo_2), and $Al_{16}Cr_{16}Fe_{33}Ni_{33}Mo_3$ (Mo_3) (at.–%). An industrial superduplex steel 1.4517 (DIN EN 10283/ASTM A890) is included as reference material. The research is embedded in a targeted European effort aiming at applications, which require a good balance between strength, ductility, and toughness along with wear and corrosion resistance in areas commonly served by duplex and superduplex steels. In this paper, we present and discuss the contribution of molybdenum to phase stability and describe the effects of annealing heat treatments on microstructure and selected mechanical properties. Main attention is given to alloys Mo_0 and Mo_2.

EXPERIMENTAL PROCEDURES

We investigated samples with an ultrafine vermicular duplex microstructure in a series of alloys $AlCrFe_2Ni_2Mo_x$ (molar ratio) starting from the initial composition $AlCrFe_2Ni_2$. Molybdenum additions ranged from $x = 0.06$ to 0.18 molar ratio, corresponding to 1–3 at.–%. Samples were produced by arc melting (Edmund Bühler AM500) of large 300 g buttons from raw elemental metals with a purity above 99.8 wt.–%. The samples were molten under 0.7 bar argon (purity 5.0) with a Ti-getter after having evacuated the chamber to 10^{-5} bar followed by repeated purging with argon to prevent oxygen pickup. The samples were then flipped and remolten three times to ensure chemical homogeneity. **Table 1** shows the nominal and measured alloy compositions as determined by energy dispersive x-ray spectrometry (EDS).

The arc-melted buttons were cut by wire electrical discharge machining (Excetek V400G) to produce specimens for microstructure characterization and instrumented micro-indentation before and after defined annealing treatments. Furthermore, from the samples, Mo_0 and Mo_2 rectangular specimens with the dimensions $30 \times 5 \times 1.6$ mm were extracted for 3-point-bending tests and subjected to annealing heat treatments at 950°C for 6 h followed by water quenching. Moreover, specimens from Mo_2 were annealed at 1100°C for varying holding times, that is, 10 min to 3 h followed by water quenching. Annealing was carried out in a horizontal tube furnace (Nabertherm RHTC 80-230/15) under argon flow.

Sample preparation for microstructure analysis consisted of standard metallographic grinding and polishing steps with a final polishing step in a vibromet device (Buehler VibroMet^{TM}). Samples were analyzed in scanning electron microscopes (Zeiss, Gemini Ultra 55 and Gemini Leo 1550) equipped with detectors for EDS analysis (Oxford Instruments X-max 150) and electron backscatter diffraction (EBSD) (Nordlys HKL). Micro-indentation measurements were performed in an Anton Paar MHT^3 using a Vickers indenter at a loading speed of 2000 mN/min and a maximum load of 500 mN. The 3-point-bending tests were carried out in a miniature testing device (MTI SEMtester 1000 EBSD) using a constant displacement of 0.2 mm/min (strainrate $\sim$0.3% s^{-1}) until a maximum strain of 20% or sample failure was reached. For improved statistics three to five specimen were tested per alloy composition and annealing condition.

EXPERIMENTAL RESULTS AND DISCUSSION

In section "Microstructure Characterisation," we describe the microstructure in the arc melted condition and after annealing heat treatments with focus on morphological and crystalline features of the dual phase structure, the phase fractions, and compositions. In section "Mechanical Properties," we present

TABLE 1 | Nominal and integral composition of fabricated $AlCrFe_2Ni_2Mo_x$ samples by EDS (at.%).

Alloy	Nominal composition	Chemical composition by EDS in at.%				
		Al	Cr	Fe	Ni	Mo
Mo_0	$Al_{17}Cr_{17}Fe_{33}Ni_{33}$	17.1 ± 0.1	16.9 ± 0.1	32.6 ± 0.3	33.3 ± 0.4	–
Mo_1	$Al_{17}Cr_{17}Fe_{33}Ni_{33}Mo_1$	16.3 ± 0.1	17.1 ± 0.1	32.5 ± 0.2	33.0 ± 0.1	1.0 ± 0.1
Mo_2	$Al_{16}Cr_{16}Fe_{33}Ni_{33}Mo_2$	16.1 ± 0.1	17.0 ± 0.1	32.8 ± 0.1	32.2 ± 0.1	2.0 ± 0.1
Mo_3	$Al_{16}Cr_{16}Fe_{33}Ni_{33}Mo_3$	16.0 ± 0.1	17.0 ± 0.1	32.3 ± 0.2	31.7 ± 0.1	3.0 ± 0.1

EDS measurements were performed on five randomly placed areas on the sample and the values represent the mean and standard deviation of the five measurements.

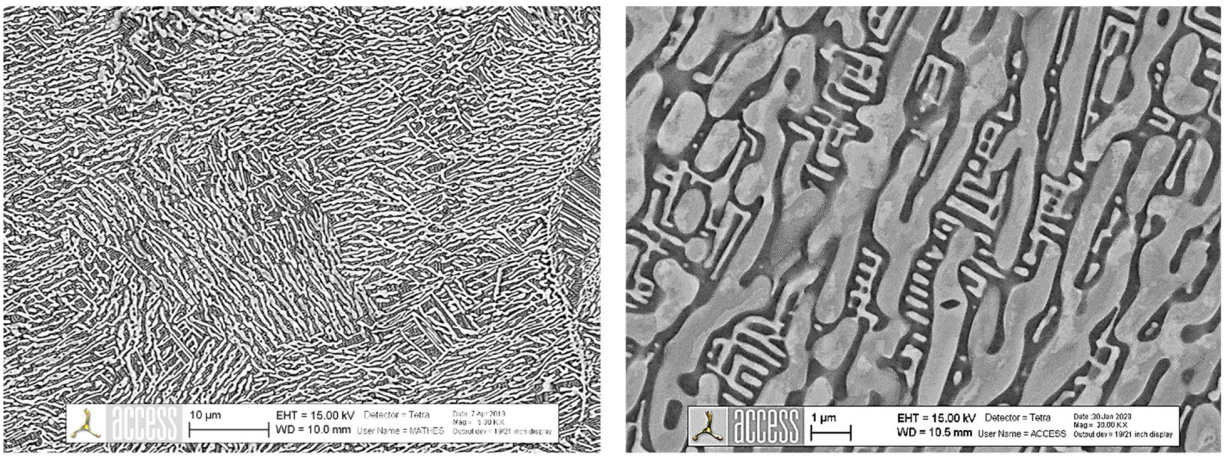

FIGURE 1 | SEM-BSE micrographs of the as-cast microstructure in sample Mo_2 **(A)** displays a low magnifcation overview while **(B)** shows the ultrafine vermicular duplex structure with the FCC phase (bright) closely entangled with the spinodal decomposed BCC phase (dark).

the mechanical properties from micro-indentation and 3-point-bending, respectively.

Microstructure Characterization

Initial Condition After Arc Melting

Figure 1 – shows an overview of the microstructure in the initial "as-cast" condition of the Mo_2 sample at different magnifications, which allows identifying the multiscale structural features as follows: **Figure 1A** – At low magnifications, one distinguishes large dual-phase grains, which are former (parent) BCC-B2 grains. **Figure 1B** – Inside the grains, an ultrafine vermicular FCC phase is present (bright color), while the BCC matrix is spinodally decomposed at nanoscale. The decomposition products are BCC-B2#2 (dark) and BCC-A2# (bright). The vermicular FCC and the spinodal BCC are visibly entangled, the FCC phase fraction reaching about 60 area–%. Two types of boundaries are visible (i) grain boundaries, decorated by a continuous film of FCC and (ii) domain boundaries, which separate regions of similar FCC directionality, being in fact boundaries between crystallographic FCC variants. Sometimes, grain boundaries show small regions with Widmanstätten rather than vermicular FCC. These features are similar to those reported by Dong et al. for the Mo-free alloy $AlCrFe_2Ni_2$; however, Mo additions greatly reduce the extent of Widmanstätten regions. Hecht et al. discuss more details about the competition between Widmanstätten and vermicular FCC in this Frontier's edition, "The BCC-FCC phase transformation pathways and crystal orientation relationships in dual phase materials from Al-(Co)-Cr-Fe-Ni alloys."

Molybdenum additions, even in small quantities, have a pronounced effect on the FCC phase fraction formed upon continuous cooling through the BCC→FCC phase transformation, but also on the morphological anisotropy. **Figure 2** displays high magnification micrographs of the as-cast microstructure in the four alloys Mo_0 through Mo_3. The FCC phase fraction evaluated by image analysis ranges from 50% in Mo_0, 60% Mo_1 and Mo_2 and finally 45% in Mo_3. This is surprising, because Mo is a BCC stabilizing element. The increase of the FCC fraction from 50 to 60% seems counterintuitive but relates to the fact that Mo additions implicitly decrease the aluminum content, simply by dilution. This indicates that Mo is a less strong BCC stabilizing element compared with Al. Only above 2 at.–% Mo, for example, in Mo_3, the BCC stabilizing effect of Mo compensates for the dilution of Al, thus leading to a decrease of the FCC phase fraction to 45%.

From **Figure 2**, it is perceivable that molybdenum additions lead to an increasing microstructural anisotropy, both regarding the directionality of the vermicular FCC structure but also regarding the nanoscale pattern inside the spinodally

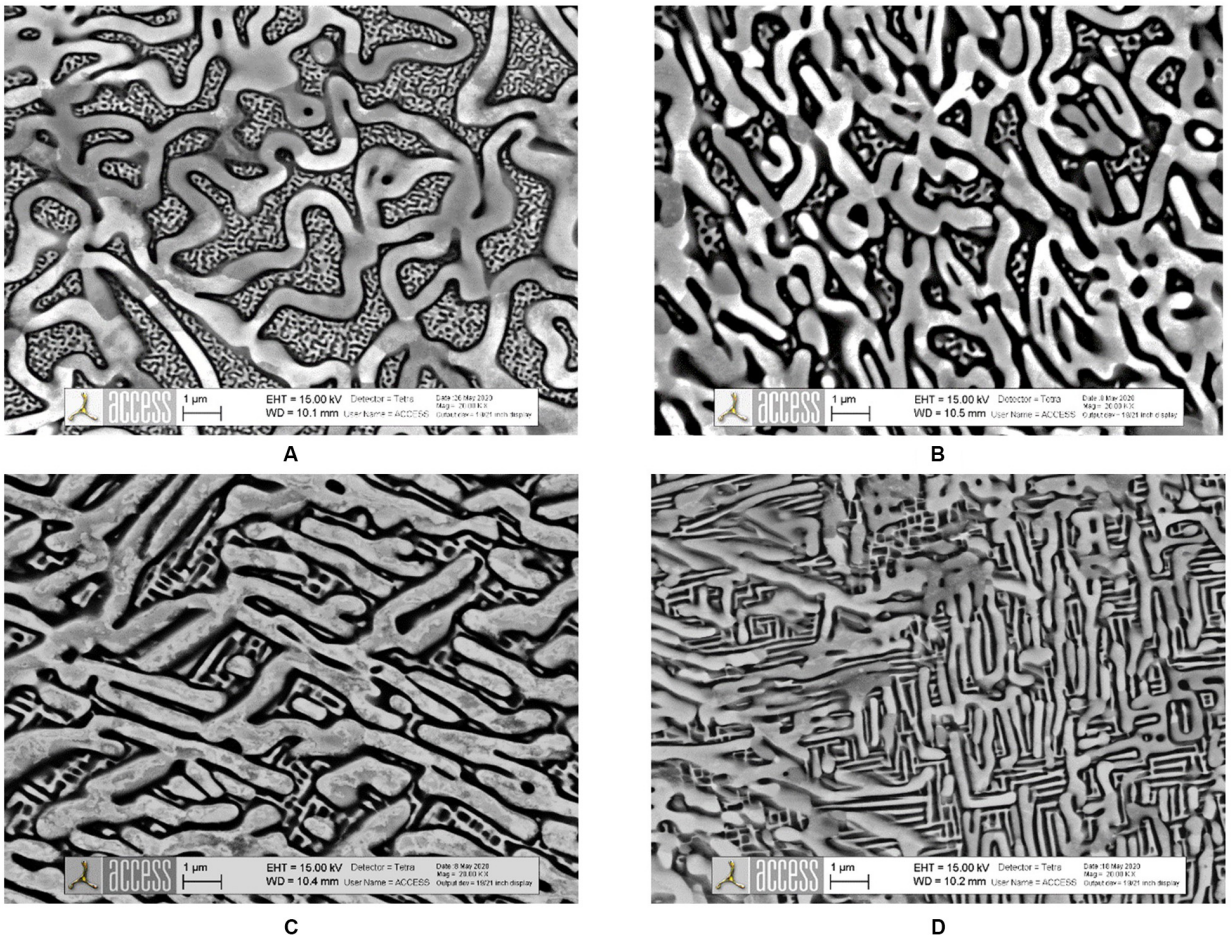

FIGURE 2 | SEM-BSE images of the ultrafine vermicular duplex structure in as-cast Mo_x samples, showing increasing morphological anisotropie with increasing Mo: **(A)** Mo-free, **(B)** 1 Mo, **(C)** 2 Mo, and **(D)** 3 Mo (at.-%).

TABLE 2 | Morphological and crystallographic features of the FCC phase in of Mo_0 and Mo_2: Phase fraction, average thickness, average and 95th percentile intergranular misorientation.

Sample	FCC phase fraction (%)	Average thickness (μm)	Intergranular misorientation (°)	
			Average	95th percentile
Mo_0 as-cast	52 ± 0	0.54 ± 0.03	5.2 ± 2.5	8.8
Mo_0 950°C 6 h	58 ± 2	0.89 ± 0.18	4.0 ± 2.0	8.0
Mo_2 as-cast	59 ± 2	0.48 ± 0.09	4.9 ± 2.2	9.5
Mo_2 950°C 6 h*	44 ± 1	0.86 ± 0.14	4.4 ± 1.8	7.9
Mo_2 1100°C 10 min	58 ± 1	0.79 ± 0.14	5.7 ± 2.5	10.3
Mo_2 1100°C 1 h	60 ± 3	1.09 ± 0.12	4.0 ± 1.9	7.8
Mo_2 1100°C 2 h	56 ± 1	1.13 ± 0.17	4.6 ± 2.2	8.6
Mo_2 1100°C 3 h	57 ± 1	1.31 ± 0.14	5.3 ± 2.6	10.4

**Sigma phase 17%; Composition by EDS in at.%: Al 4.7 ± 1.0 Cr 36.2 ± 0.9 Fe 39.9 ± 0.8 Ni 11.8 ± 0.9 Mo 7.5 ± 0.3.*

decomposed BCC phase. The increased anisotropy is attributed to an increase of the BCC-A2 phase fraction inside the spinodal structure but likely also to an increase of the interfacial energy anisotropy. The simulation study by Vidyasagar et al. (2018) illustrates the importance of interfacial energy anisotropy during spinodal decomposition.

Table 2 lists all measured quantitative data regarding the FCC phase fraction and the average thickness of the FCC vermicelli, also including the lattice strain observed by EBSD and analyzed by the MTEX software. Indeed, the EBSD analysis of the ultrafine vermicular samples in the as-cast as well as annealed conditions revealed that the FCC phase is significantly strained, containing a

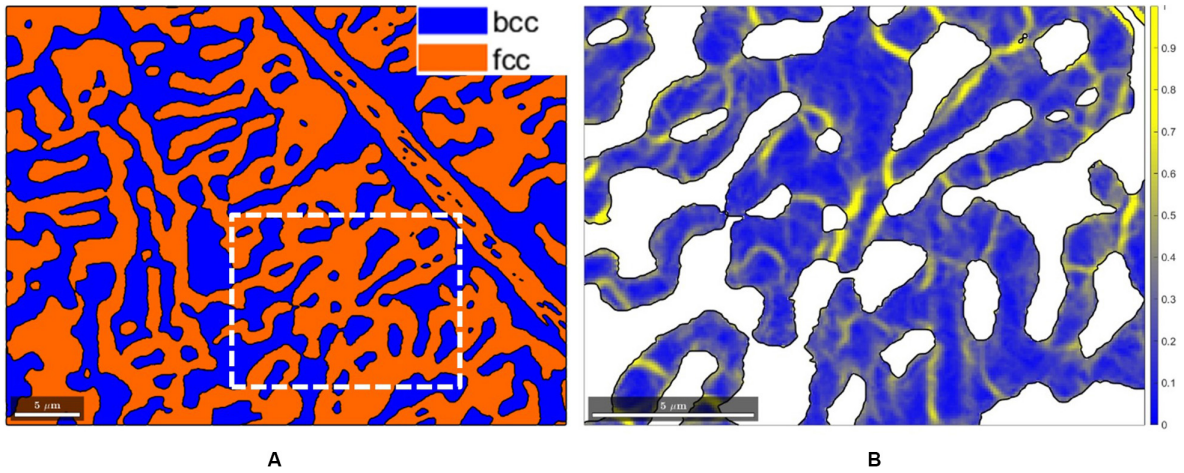

FIGURE 3 | (A) EBSD Phase map of Mo_2 after annealing at 1100°C for 3 h and **(B)** magnified region with a map of the kernel average misorientation within the FCC phase.

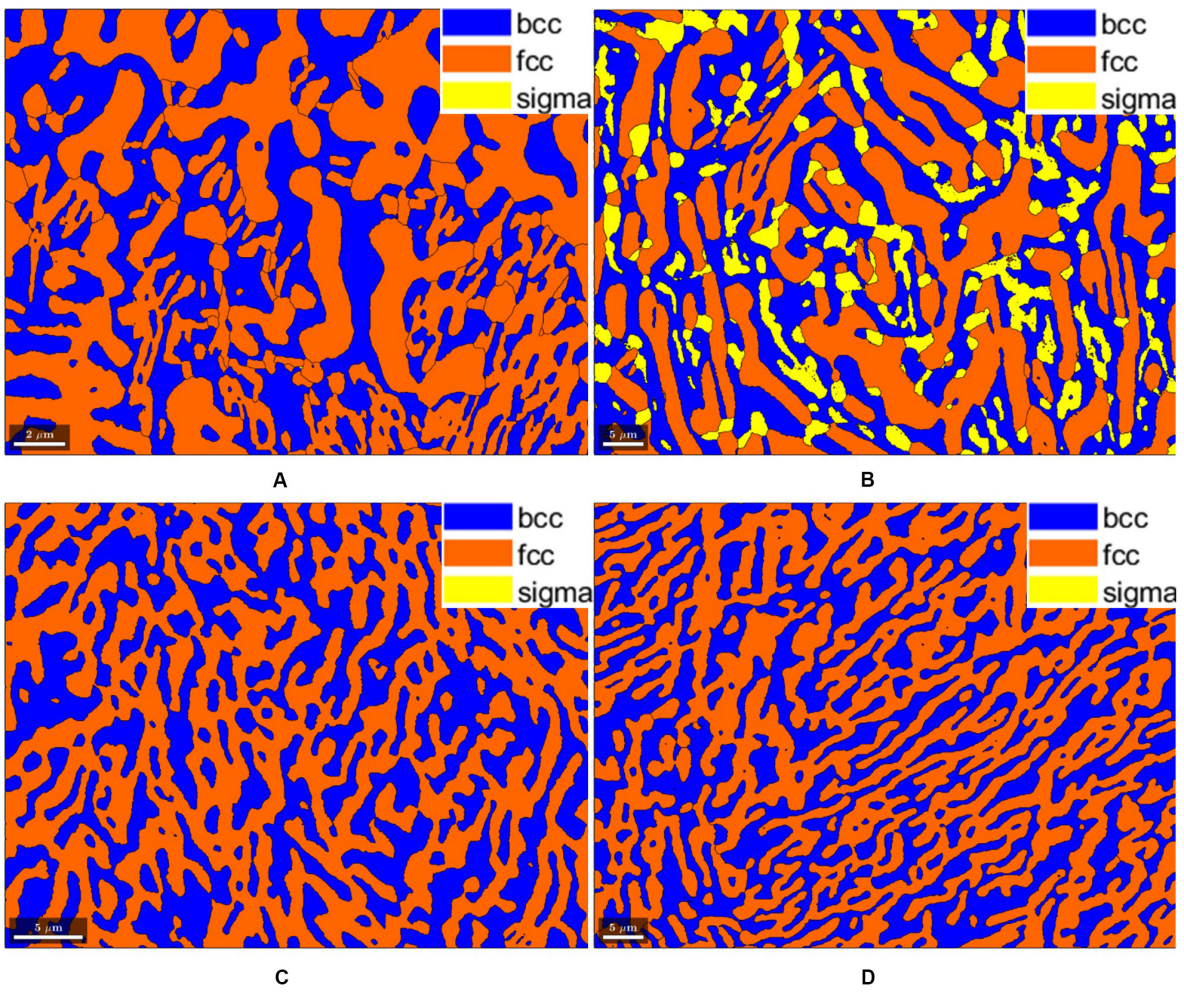

FIGURE 4 | EBSD map of samples **(A)** Mo_0 in as-cast condition, **(B)** Mo_2 after annealing at 950°C/6 h, **(C)** after annealing at 1100°C/1 h, and **(D)** 1100°C/3 h. Sigma phase is only present in Mo_2 950°C/6 h.

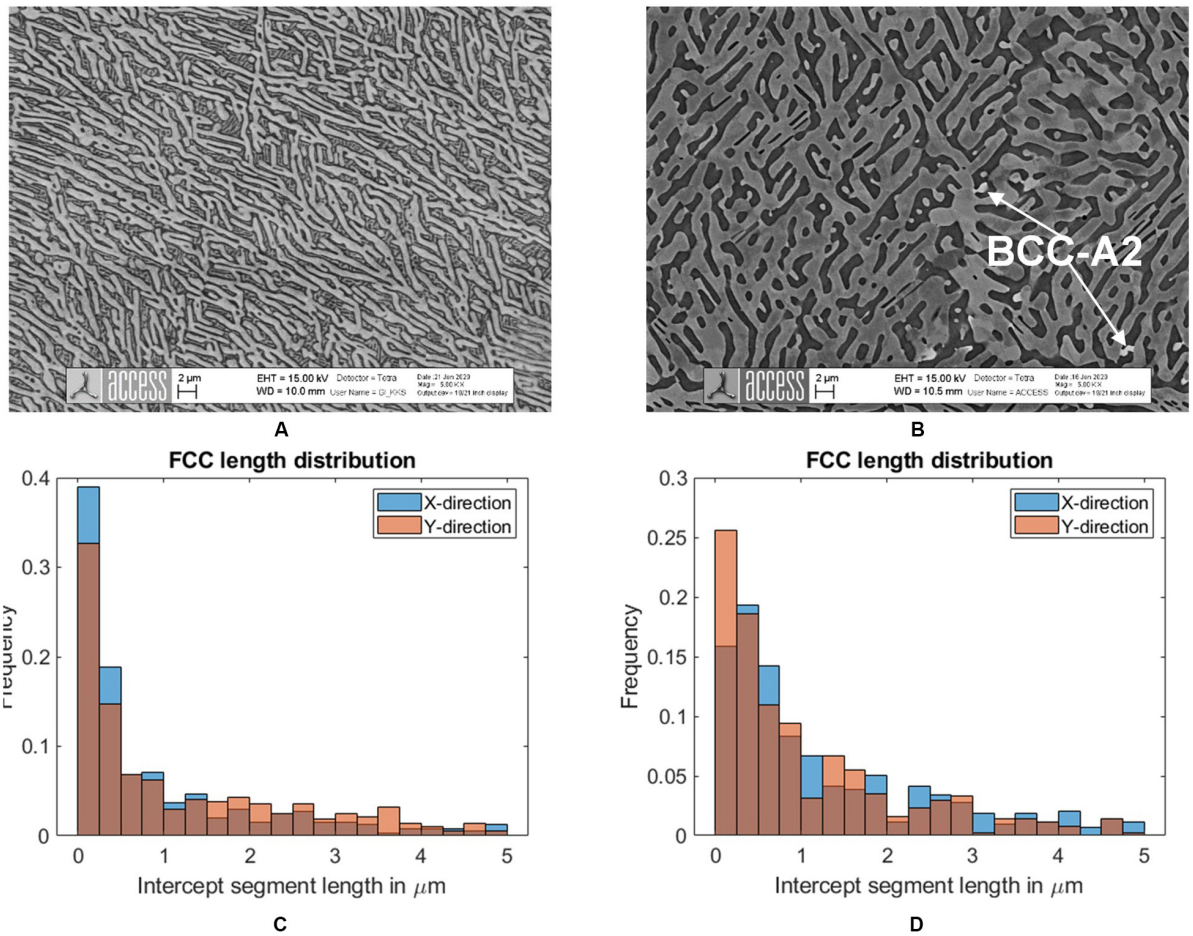

FIGURE 5 | FCC size distribution in sample Mo_2 in as-cast conditions **(A,C)** and after annealing at 1100°C for 3 h **(B,D)**. The size distribution was measured by the line intercept method using both vertical and horizontal lines.

TABLE 3 | Phase compositions in Mo_0 and Mo_2 after annealing at 1100°C/3 h measured by EDS.

AlCrFe$_2$Ni$_2$	**Al (at.%)**	**Cr (at.%)**	**Fe (at.%)**	**Ni (at.%)**	**Mo (at.%)**
FCC (A1)	5.4 ± 0.1	23.5 ± 0.2	46.5 ± 0.3	24.6 ± 0.3	–
BCC (A2)	20.7 ± 0.2	23.7 ± 1.1	27.2 ± 0.4	28.5 ± 0.8	–
BCC (B2)	30.7 ± 1.3	8.8 ± 2.7	16.3 ± 1.8	44.2 ± 3.2	–
AlCrFe$_2$Ni$_2$Mo$_{0.1}$	**Al (at.%)**	**Cr (at.%)**	**Fe (at.%)**	**Ni (at.%)**	**Mo (at.%)**
FCC (A1)	7.3 ± 0.1	22.0 ± 0	41.3 ± 0.5	26.5 ± 0.3	2.8 ± 0.1
BCC (A2)	6.9 ± 0.6	33.2 ± 0.1	41.3 ± 0.4	13.5 ± 0.3	5.1 ± 0.1
BCC (B2)	33.0 ± 0.3	5.6 ± 0.7	15.1 ± 0.7	46.0 ± 1.3	0.4 ± 0.2

high density of subgrain boundaries. The strain originates from the BCC→FCC phase transformation, which involves lattice rotation and dilatation relative to the parent BCC. **Figure 3** shows the subgrain network for sample Mo_2 after annealing at 1100°C/3 h based on the kernel average misorientation map (the average misorientation angle of a given point with all its first neighbors) plotted by MTEX. We believe that apart from classical transformation strain, the observed subgrain network relates to the growth conditions of the vermicular FCC from the initial BCC-B2 parent phase. Unlike Widmanstätten FCC plates, which grow into chemically homogeneous BCC-B2, the vermicular FCC was observed to grow into spinodally decomposing BCC-B2 (see Hecht et al. in this Frontier's edition). The compositional modulation in the parent grain is likely causing additional strain.

Annealed Condition After Isothermal Heat Treatments

Annealing heat treatments were carried out at 950°C for 6 h mainly to verify the propensity of the Mo_0 and Mo_2 alloys to

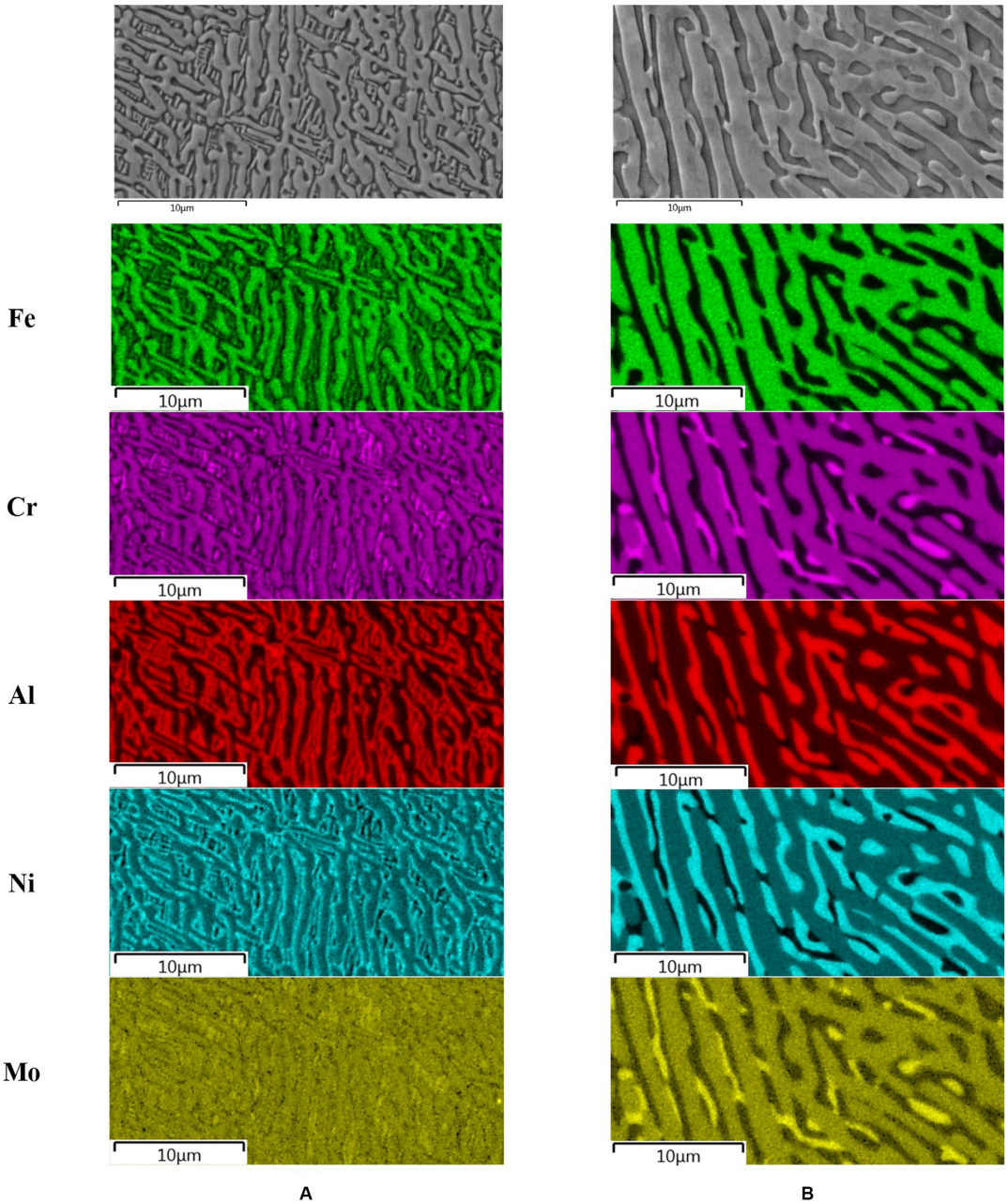

FIGURE 6 | Element distribution from EDS mapping in the sample Mo_2 for **(A)** as-cast condition and **(B)** after annealing at 1100°C for 3 h. Noteworthy is the sluggish partitioning of molybdenum in the as-cast condition, which is recovered after heat treatment.

form the brittle sigma phase (tetragonal, space group no.136). EBSD analysis shows the absence of the sigma phase in Mo_0, while in alloy Mo_2 about 17% sigma-phase is present with a composition around Al = 6 ± 2, Cr = 35 ± 2, Fe = 39 ± 1, Ni = 13 ± 2 and Mo = 7 ± 1 (at.–%). **Figure 4** displays the EBSD phase maps for (**Figure 4A**) Mo_0 950°C/6 h, (**Figure 4B**) Mo_2 950°C/6 h, (**Figure 4C**) Mo_2 1100°C/1 h, and (**Figure 4D**) Mo_2 1100°C/3 h. The sigma phase is particularly present in Mo_2 950°C/6 h at FCC phase boundaries but also in regions where former BCC-A2 was present (**Figure 4B**). Sigma phase formation can be successfully prevented, even in sample Mo_2, after annealing at 1100°C up to 3 h followed by water quenching. Such heat treatment parameters are common practice for duplex steels, even for thick section castings, to avoid sigma phase formation (Fritz, 2014; Llorca-Isern et al., 2017).

A small series of annealing treatments were performed for Mo_2 at 1100°C with distinct holding durations of 10 min, 1, 2, and 3 h, followed by water quenching. The series aimed

TABLE 4 | Overview of mechanical properties for all tested conditions for Mo_0 and Mo_2.

Sample	HV 0.05	E_{it} (GPa)	YS (0.2%) (MPa)	Flexural UTS (MPa)	Elongation at fracture (%)
Mo_0	326 ± 6	190 ± 12	1140 ± 40	2150 ± 60	16.0
Mo_0 950°C 6 h	304 ± 6	197 ± 12	1000 ± 50	2050 ± 30	14.3
Mo_2	384 ± 6	193 ± 7	1330 ± 90	2200 ± 90	15.6
Mo_2 950°C 6 h	392 ± 8	183 ± 13	1100 ± 50	1900 ± 40	4.2
Mo_2 1100°C 10 min	333 ± 8	189 ± 9	1150 ± 60	2060 ± 25	>20.0
Mo_2 1100°C 1 h	324 ± 7	189 ± 12	1020 ± 50	2040 ± 110	>20.0
Mo_2 1100°C 2 h	315 ± 7	192 ± 6	930 ± 50	1950 ± 130	>20.0
Mo_2 1100°C 3 h	315 ± 3	188 ± 10	900 ± 30	2000 ± 30	>20.0
Superduplex 1.4517	185 ± 15	155 ± 9	1110 ± 50	1620 ± 80	>20.0

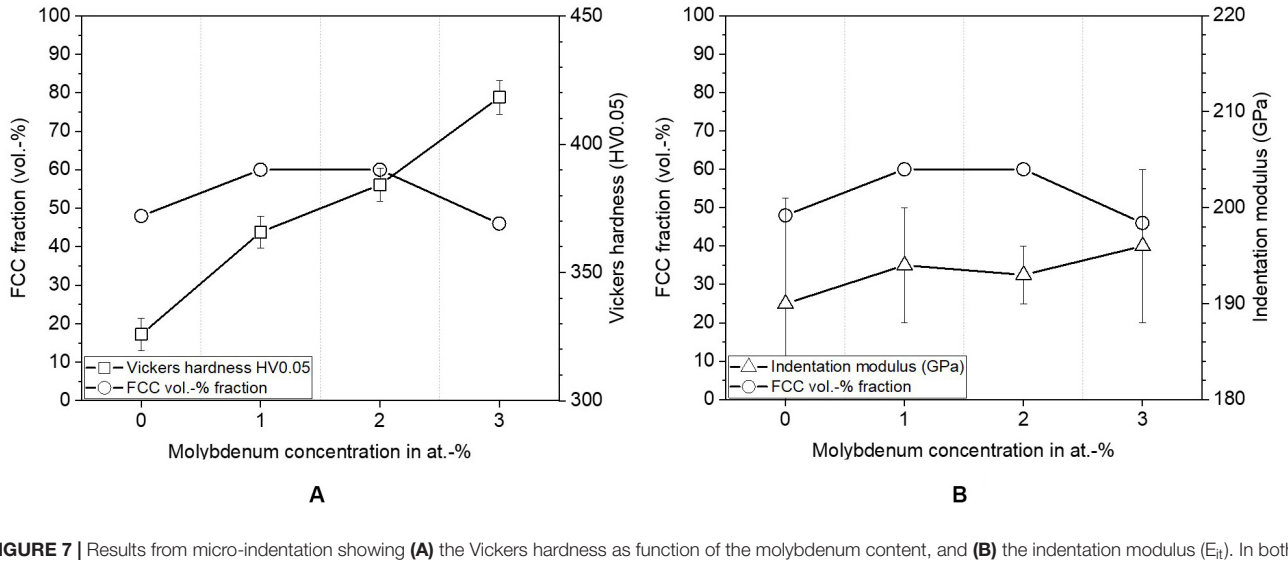

FIGURE 7 | Results from micro-indentation showing **(A)** the Vickers hardness as function of the molybdenum content, and **(B)** the indentation modulus (E_{it}). In both diagrams, the FCC phase fraction is equally plotted.

at verifying the coarsening of the ultrafine vermicular FCC phase and of the spinodal structure. **Figures 5A,B** illustrates the effects of coarsening by comparing the as-cast (**Figure 5A**) and annealed microstructures after 1100°C/3 h (**Figure 5B**). The comparison shows that the FCC phase thickens considerably, without changes in the phase fraction (see **Table 2**). The average thickness increases from 0.5 μm in the as-cast state to 1.3 μm in the annealed state. Coarsening is associated with an increasing contiguity of the FCC network. **Figures 5C,D** displays the size distribution of the FCC phase measured by the line intercept method along horizontal and vertical lines. The most dramatic coarsening is seen in the spinodal structure, which vanishes nearly completely, leaving behind few globulitic BCC-A2 particles. Without having analyzed the BCC-A2 fraction quantitatively, we qualitatively see a decrease of the BCC-A2 fraction, which is in agreement with the thermodynamics of the system. By heat treatment, the subgrain network inside the FCC phase is not changed significantly. We do not observe significant changes of the intergranular misorientation or of the low angle grain boundary distribution. **Table 2** summaries the morphological and crystallographic features of the FCC phase for Mo_0 and Mo_2 for all heat treatment conditions.

Due to coarsening, it was feasible to measure the chemical composition of the individual phases in Mo_0 and Mo_2 by EDS. **Table 3** summarizes the results. As can be seen, molybdenum partitions mainly to the BCC-A2 phase, while being <0.5 at.% in the BCC-B2 phase. The FCC phase contains 2.8 at.% Mo. EDS maps provided in **Figure 6** show the elemental partitioning between the phases for Mo_2 in the as-cast and annealed 1100°C/3 h condition. An interesting and noteworthy observation is that molybdenum partitioning occurs only during heat treatment. The as-cast sample (**Figure 6**, left column) shows a sluggish Mo-partitioning, even though the other elements are clearly partitioned. This is likely due to kinetic effects, which are commonly termed as "solute trapping," being associated to limited diffusion of Mo in BCC-B2. After heat treatment (**Figure 6**, right column), molybdenum partitioning is complete, and mainly to the BCC-A2 and the FCC-A1 phases. The Mo-content of the BCC-B2 phase is below 0.5 at.–%.

Mechanical Properties

The basic mechanical properties investigated on small samples in the as-cast and annealed states relate to results from micro-indentation and 3-point-bending, as presented below

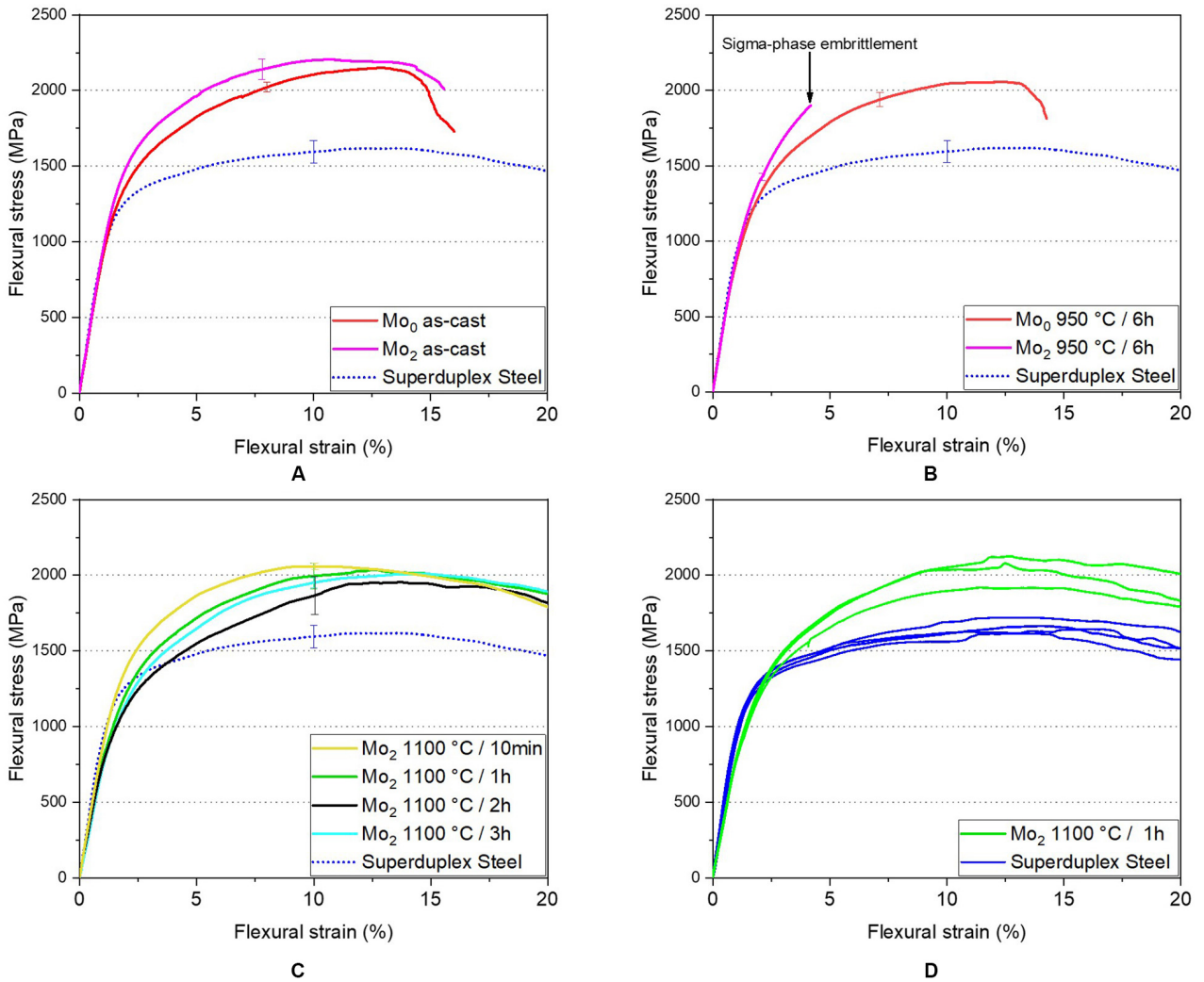

FIGURE 8 | (A) Flexural stress-strain curves in as-cast conditions: $AlCrFe_2Ni_2$ (Mo_0) in red, $AlCrFe_2Ni_2Mo_{0.1}$ (Mo_2) in magenta, superduplex steel reference 1.4517 in blue, **(B)** after annealing at 950°C/6 h: Mo_0 in red, Mo_2 in magenta, **(C)** Mo_2 after annealing at 1100°C for 10 min (yellow), 1 h (green), 2 h (black), and 3 h (light blue). Illustration of the spread shown in **(D)** for Mo_2 1100°C/1 h and the reference superduplex steel.

and summarized in **Table 4** for the Mo_0 and Mo_2 in all tested conditions.

Micro-Indentation

Figures 7A,B provide the Vickers hardness (HV0.05) and the indentation modulus (E_{it}) as function of the molybdenum content for samples in the as-cast state along with the values of the FCC phase fraction. The Vickers hardness increases markedly with increasing Molybdenum content from 326 ± 6 HV0.05 in Mo_0 to 418 ± 7 HV0.05 in Mo_3, independent of the BCC/FCC phase ratio. The origin of this increase may relate to increased density and bulk modulus of the alloy as was reported by Ledbetter et al. for the Fe-Cr-Ni system (Ledbetter and Austin, 1988; Ledbetter and Kim, 1988). However, we remind the microstructure observations (compare **Figure 2**), which showed that Mo increases the BCC-A2 phase fraction inside the spinodal BCC, leading to a plate-like morphology. At this stage, the quantitative analysis of the BCC-A2 fraction is still pending. As shown in **Figure 7B**, the indentation modulus increases only slightly from 190 to 196 GPa.

The evolution of hardness and indentation modulus for the annealed samples (Mo_0 and Mo_2) are listed in **Table 4** along with results from 3-point-bending. As expected, upon annealing the hardness decreases with increasing temperature and/or annealing time. The lowest hardness of around 315 HV0.05 is reached in Mo_2 after annealing at 1100°C for 3 h, which is still significantly higher than the hardness of the reference superduplex steel 1.4517 with 185 HV0.05.

Three-Point Bending Tests

Three-point-bending tests of miniature specimens 30 × 5 × 1.6 mm reveal the potential of the alloy Mo_2 for applications as structural material compared to the reference superduplex steel. Furthermore, the tests also shed light on means

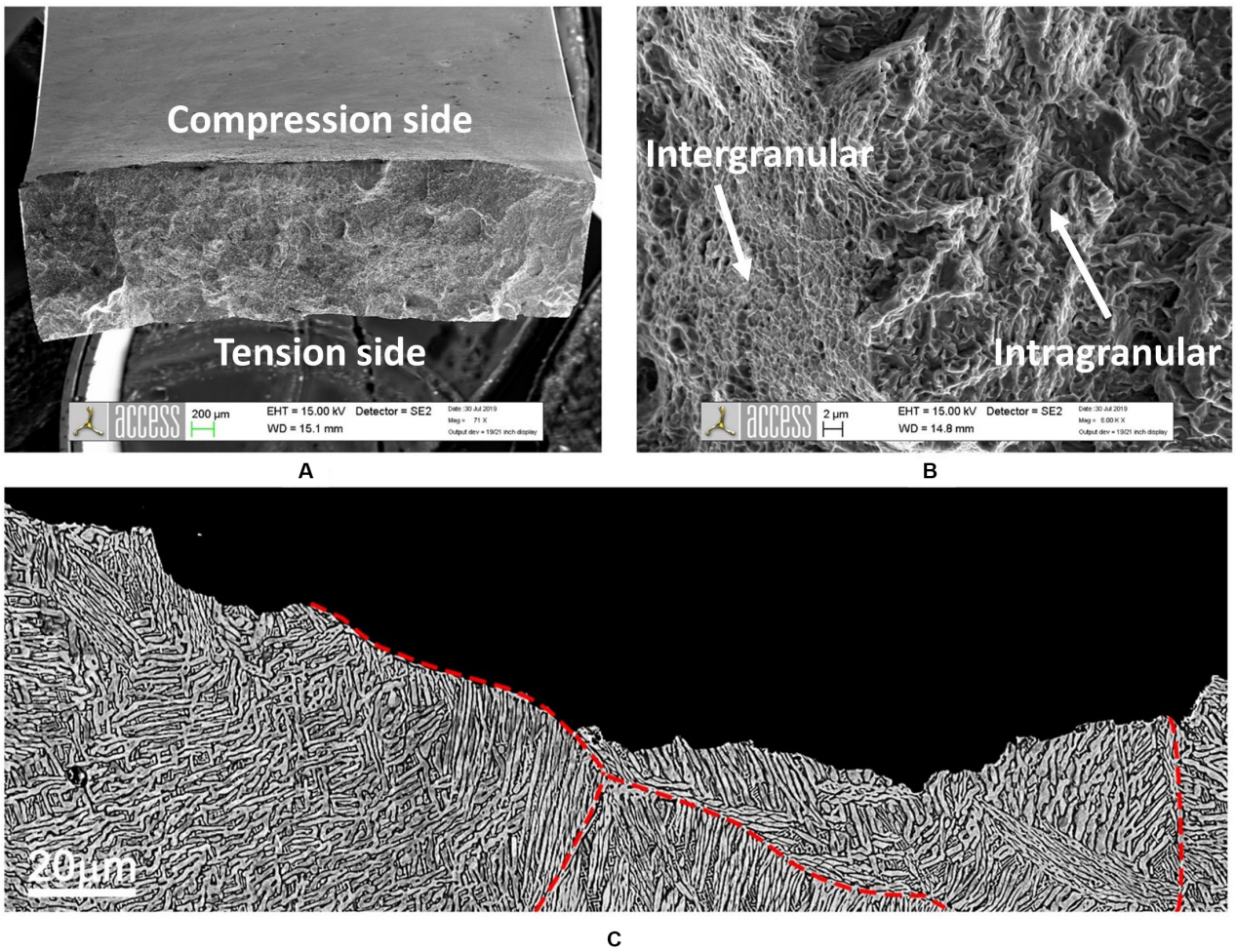

FIGURE 9 | Overview SEM-SE image of an as-cast Mo_2 specimen fractured surface in **(A),** in **(B)** a high magnification fracture surface image with (left) an intergranular fracture region and (right) an intragranular fracture region. **(C)** shows a perpendicular metallographic section plane of the fracture surface with (red strokes) outlined grain boundaries.

of balancing strength and ductility by annealing treatments. The main results are shown in **Figure 8** as follows: **Figure 8A** compares the as-cast Mo_0 and Mo_2 samples to the as received and heat treated (1150°C for 3 h) superduplex steel 1.4517. Both alloys show pronounced and similar strain hardening, with the Mo-containing Mo_2 being slightly stronger than the Mo-free Mo_0. Both materials outpace the superduplex steel in terms of maximum flexural strength, however at the expense of ductility. The ductility is none the less considerably high, reaching about 15% flexural strain at fracture. **Figure 8B** compares the Mo_0 and Mo_2 in the heat-treated condition 950°C/6 h and reveals the embrittlement by sigma phase in the Mo_2 sample. **Figure 8C** compares distinct annealing durations at 1100°C for Mo_2 samples and shows that the yield strength decreases with increasing annealing durations, while the ductility increases significantly to flexural stains above 20%. The flexural UTS remains as high as 2000 MPa compared to 1600 MPa of the superduplex reference steel, while the yield stress falls down to the level of the reference steel. In all above figures, the plotted stress-strain curves are averaged over 3 to 5 tested specimens. **Figure 8D** illustrates the spread, taking as representative example all tested Mo_2 specimens annealed at 1100°C/1 h as well as the reference steel. All specimens reach the flexural strain of 20% being the limit of the testing device.

Further, the fracture surface of one as-cast Mo_2 specimen, failed during bending, was inspected in SEM as well as in a metallographic section plane placed perpendicular to the fracture surface. We identified both, inter- and intragranular fracture paths, as shown in **Figure 9**. In **Figure 9A**, we outline the grain boundaries to highlight that a part of the fracture path follows a grain boundary. Grain boundaries are decorated by a thin layer of FCC phase. **Figure 9B** displays a SEM-SE view of the fractures specimen with labels indicating the tensile and compression side. Finally, **Figure 9C** shows a high magnification of the fracture surface including a region of intergranular fracture on the left side and a region with intragranular fracture on the right side.

Taken together, the bending results clearly prove a remarkable strain hardening capability of the investigated alloys, which

is indeed one of the most prominent properties of HEAs as already discussed by Wang and Misra (2011) and Basu et al. (2018). Current work is directed toward better understanding the strain partitioning between BCC and FCC phases and identify the mechanisms behind strain hardening. Furthermore, the vermicular and highly contiguous microstructure is expected to show attractive fatigue properties, which are currently investigated. The hardness values, which outpass the superduplex steel by far, may improve the wear resistance, while calling for a careful investigation of the impact toughness.

SUMMARY AND CONCLUSION

We have investigated the effects of minor additions of molybdenum to the medium entropy alloy $AlCrFe_2Ni_2$ regarding the microstructure and basic mechanical properties with focus on annealing heat treatments. The alloy develops an ultrafine vermicular microstructure composed of 60% FCC and 40% BCC, the BCC being spinodally decomposed into BCC-A2 + BCC-B2. The vermicular microstructure displays a high contiguity, the phases forming a neatly entangled network. The following main conclusions are drawn:

- The ultrafine vermicular microstructure formed in the Mo-free baseline alloy $AlCrFe_2Ni_2$ is retained for Mo additions up to 3 at.%; however the directionality of the FCC phase increases, as does the anisotropy of the spinodal pattern. The latter is attributed to an increasing fraction of the BCC-A2 phase but may also relate to stronger interfacial anisotropy between the product phases of the spinodal decomposition.
- The FCC phase in the ultrafine vermicular microstructure displays significant strain and a network of low angle grain boundaries. The average intragranular misorientation does not change significantly during annealing treatments.
- Alloy Mo_2 with 2 at.% Mo is prone to sigma formation and related embrittlement. Annealing heat treatments must exceed the stability limit of the sigma phase, that is, ∼1000°C. At 950°C the sigma fraction is as high as 17%. Annealing at 1100°C safely avoids sigma formation.
- Alloy Mo_2 with 2 at.% Mo shows promising mechanical properties, which can be balanced by annealing at 1100°C. With increasing annealing duration, the ductility (flexural strain) increases at the expense of the yield strength. The ultimate flexural strength remains nearly unchanged at ∼2000 MPa, well exceeding the strength of the reference superduplex steel 1.4517. Like all investigated medium and HEAs, Mo_2 shows a remarkable strain hardening behavior, expected to prove beneficial to the wear resistance.
- An annealing treatment at 1100°C for the duration of 30 min to 1 h with subsequent water quenching is recommended.

DATA AVAILABILITY STATEMENT

The raw data supporting the conclusions of this article will be made available by the authors, without undue reservation, to any qualified researcher.

AUTHOR CONTRIBUTIONS

SG designed the study, performed all the experiments and analyzed the experimental results as part of his Ph.D. research. VW performed the thermodynamic calculations which guided the selection of annealing conditions. UH supervised the research and contributed to the process of writing the manuscript. All authors contributed to the article and approved the submitted version.

FUNDING

The German Federal Ministry for Education and Research (BMBF) supported this research under Grant No. 03XP0163A in the frame of the M-era.Net Joint Call 2017, Project NADEA (No. 5129).

ACKNOWLEDGMENTS

We kindly thank Otto Junker GmbH for providing the superduplex steel EN 1.4517 (ASTM A890 Grade 1B) in the cast and fully heat-treated condition to serve as reference material.

REFERENCES

Abuzaid, W., and Sehitoglu, H. (2018). Plastic strain partitioning in dual phase Al13CoCrFeNi high entropy alloy. *Mater. Sci. Eng. A* 720, 238–247. doi: 10.1016/j.msea.2018.02.044

Alvarez-Armas, I., and Degallaix-Moreuil, S. (eds) (2013). *Duplex Stainless Steels*. Hoboken, NJ: John Wiley & Sons Inc, doi: 10.1002/9781118557990

Basu, I., Ocelík, V., and De Hosson, J. T. M. (2018). BCC-FCC interfacial effects on plasticity and strengthening mechanisms in high entropy alloys. *Acta Mater.* 157, 83–95. doi: 10.1016/j.actamat.2018.07.031

Bönisch, M., Wu, Y., and Sehitoglu, H. (2018). Twinning-induced strain hardening in dual-phase FeCoCrNiAl0.5 at room and cryogenic temperature. *Sci. Rep.* 8, 1–9. doi: 10.1038/s41598-018-28784-1

Dong, Y., Gao, X., Lu, Y., Wang, T., and Li, T. (2016). A multi-component AlCrFe2Ni2 alloy with excellent mechanical properties. *Mater. Lett.* 169, 62–64. doi: 10.1016/j.matlet.2016.01.096

Dong, Y., Lu, Y., Kong, J., Zhang, J., and Li, T. (2013). Microstructure and mechanical properties of multi-component AlCrFeNiMo x high-entropy alloys. *J. Alloys Compd.* 573, 96–101. doi: 10.1016/j.jallcom.2013.03.253

Eleno, L., Frisk, K., and Schneider, A. (2006). Assessment of the Fe-Ni-Al system. *Intermetallics* 14, 1276–1290. doi: 10.1016/j.intermet.2005.11.021

Fritz, J. D. (2014). "Heat treating of austenitic and duplex stainless steels[1]," in *Heat Treating of Irons and Steels*, eds J. L. Dossett and G. E. Totten (Cleveland, OH: ASM International), 370–381. doi: 10.31399/asm.hb.v04d.a0005990

Gwalani, B., Gangireddy, S., Zheng, Y., Soni, V., Mishra, R. S., and Banerjee, R. (2019). Influence of ordered L1 2 precipitation on strain-rate dependent

mechanical behavior in a eutectic high entropy alloy. *Sci. Rep.* 9, 1–13. doi: 10.1038/s41598-019-42870-y

Hsu, C. Y., Wang, W. R., Tang, W. Y., Chen, S. K., and Yeh, J. W. (2010). Microstructure and mechanical properties of new AlCoxCrFeMo 0.5Ni high-entropy alloys. *Adv. Eng. Mater.* 12, 44–49. doi: 10.1002/adem.200900171

Jönsson, B. (1995). Assessment of the mobilities of Cr, Fe and Ni in bcc Cr-Fe-Ni Alloys. *ISIJ Int.* 35, 1415–1421. doi: 10.2355/isijinternational.35.1415

Kozak, R., Sologubenko, A., and Steurer, W. (2015). Single-phase high-entropy alloys – an overview. *Zeitschrift. Krist.* 230, 55–68. doi: 10.1515/zkri-2014-1739

Langer, J. (1971). Theory of spinodal decomposition in alloys. *Ann. Phys.* 65, 53–86. doi: 10.1016/0003-4916(71)90162-X

Ledbetter, H. M., and Austin, M. W. (1988). Molybdenum effect on volume in Fe-Cr-Ni alloys. *J. Mater. Sci.* 23, 3120–3124. doi: 10.1007/BF00551282

Ledbetter, H. M., and Kim, S. A. (1988). Molybdenum effect on Fe—Cr—Ni-alloy elastic constants. *J. Mater. Res.* 3, 40–44. doi: 10.1557/JMR.1988.0040

Li, C., Qu, Y., Zhang, Y., Lv, Q., and Qi, H. (2020). Effect of deep cryogenic treatment on the microstructure and mechanical properties of AlCrFe2Ni2 High-entropy alloy. *Mater. Res. Express* 7:36504. doi: 10.1088/2053-1591/ab7a5f

Li, Z., You, J., Guo, Y., Li, C., Zhang, Y., and Liu, Z. (2020). Phase transition mechanism and mechanical properties of AlCrFe 2 Ni 2 High-entropy alloys with changes in the applied carbon content. *Adv. Eng. Mater.* 22:1901363. doi: 10.1002/adem.201901363

Llorca-Isern, N., López-Jiménez, I., López-Luque, H., Biezma, M. V., and Roca, A. (2017). Study of the precipitation of secondary phases in duplex and superduplex stainless steel. *Mater. Sci. Forum* 879, 2537–2542. doi: 10.4028/www.scientific.net/msf.879.2537

Misra, A., and Gibala, R. (1997). Room-temperature deformation behavior of directionally solidified multiphase Ni-Fe-Al alloys. *Metall. Mater. Trans. A Phys. Metall. Mater. Sci.* 28, 795–807. doi: 10.1007/s11661-997-1007-4

Steurer, W. (2020). Single-phase high-entropy alloys – A critical update. *Mater. Charact.* 162:110179. doi: 10.1016/j.matchar.2020.110179

Tkaczyk, A. H., Bartl, A., Amato, A., Lapkovskis, V., and Petranikova, M. (2018). Sustainability evaluation of essential critical raw materials: cobalt, niobium, tungsten and rare earth elements. *J. Phys. D. Appl. Phys.* 51:aaba99. doi: 10.1088/1361-6463/aaba99

Vidyasagar, A., Krödel, S., and Kochmann, D. M. (2018). Microstructural patterns with tunable mechanical anisotropy obtained by simulating anisotropic spinodal decomposition. *Proc. R. Soc. A Math. Phys. Eng. Sci.* 474:535. doi: 10.1098/rspa.2018.0535

Wang, J., and Misra, A. (2011). An overview of interface-dominated deformation mechanisms in metallic multilayers. *Curr. Opin. Solid State Mater. Sci.* 15, 20–28. doi: 10.1016/j.cossms.2010.09.002

Wróbel, J. S., Nguyen-Manh, D., Lavrentiev, M. Y., Muzyk, M., and Dudarev, S. L. (2015). Phase stability of ternary fcc and bcc Fe-Cr-Ni alloys. *Phys. Rev. B Condens. Matter Mater. Phys.* 91:108. doi: 10.1103/PhysRevB.91.024108

Zhu, J. M., Fu, H. M., Zhang, H. F., Wang, A. M., Li, H., and Hu, Z. Q. (2010). Microstructures and compressive properties of multicomponent AlCoCrFeNiMox alloys. *Mater. Sci. Eng. A* 527, 6975–6979. doi: 10.1016/j.msea.2010.07.028

Conflict of Interest: The authors declare that the research was conducted in the absence of any commercial or financial relationships that could be construed as a potential conflict of interest.